

Structure formation in warm dark matter cosmologies Top-Bottom Upside-Down

Sinziana Paduroiu^{1*}, Yves Revaz², Daniel Pfenniger¹

¹*Geneva Observatory, University of Geneva, CH-1290 Sauverny, Switzerland*

²*Laboratoire d'Astrophysique, École Polytechnique Fédérale de Lausanne (EPFL), 1290 Sauverny, Switzerland*

24 June 2015

ABSTRACT

The damping on the fluctuation spectrum and the presence of thermal velocities as properties of warm dark matter particles like sterile neutrinos imprint a distinct signature found from the structure formation mechanisms to the internal structures of halos. Using warm dark matter simulations we explore these effects on the structure formation for different particle energies and we find that the formation of structure is more complex than originally assumed, a combination of top-down collapse and hierarchical (bottom-up) clustering on multiple scales. The degree on which one scenario is more prominent with respect to the other depends globally on the energy of the particle and locally on the morphology and architecture of the analyzed region. The presence of shells and caustics in warm dark matter halos is another important effect seen in simulations. Furthermore we discuss the impact of thermal velocities on the structure formation from theoretical considerations as well as from the analysis of the simulations. We re-examine the assumptions considered when estimating the velocity dispersion for warm dark matter particles that have been adopted in previous works for more than a decade and we give an independent estimation for the velocities. We identify some inconsistencies in previous published results. The relation between the warm dark matter particle mass and its corresponding velocity dispersion is strongly model dependent, hence the constraints on particle mass from simulation results are weak. Finally, we review the technical difficulties that arise in warm dark matter simulations along with possible improvements of the methods.

Key words:

Dark matter: N-body simulations – galaxies, warm dark matter, structure formation.

1 INTRODUCTION

Independent studies and observations of both small and large scale structure are presently challenging the otherwise widely embraced CDM model. The so-called missing satellites problem (e.g. Klypin et al. 1999; Moore et al. 1999), where observations of galaxies do not map the abundance of substructures that are produced in CDM cosmologies is a serious drawback of the model. Furthermore, at smaller scales, the density profiles of galaxies show large cores (e.g. de Blok et al. 2001; Salucci et al. 2012; Kuzio de Naray & Kaufmann 2011) that have not been reproduced by the simulations. The failure to replicate in CDM simulations pure bulgeless galaxies which are observed in an important fraction (Kormendy et al. 2010) adds to the problem.

While several recipes have been proposed in the attempt of ameliorating these issues (e.g. Navarro et al. 1996; Mar-

tizzi et al. 2013; Mashchenko et al. 2008; Pontzen & Governato 2012), most of them introducing baryonic physics processes, current studies conclude that even including repeated baryonic outflows, large cored galaxies are not found in the simulations (Marinacci et al. 2014), although this is still highly debated in the literature.

The aforementioned situations, where the CDM model proves deficient in explaining the observations, are demanding further investigation. The WDM models, with sterile neutrinos leading as most probable particle candidates have been well studied and discussed in the literature in the past thirty years with an increased interest in the last few years (see the highlights of Daniel Chalonge workshops and Colloquiums 2011-2013 for latest developments in the WDM field (de Vega & Sanchez 2011; de Vega, Falvela & Sanchez 2012)).

It has been shown recently (Destri, de Vega & Sanchez 2012) that modeling the quantum pressure of fermionic particles (Weinberg 1962; Muccione & Pfenniger 2006) on the

* E-mail: sinziana.paduroiu@unige.ch

other hand, one can reproduce the expected cores in dwarf galaxies, known to be dark matter dominated.

Moreover, the recent detection (Bulbul et al. 2014; Boyarsky et al. 2014) of a 3.55 keV unidentified emission line both on the data from XMM spectrum of galaxy clusters and Chandra can be a hint of sterile neutrino decay.

Since particles in warm dark matter models have different intrinsic properties from the cold dark matter particle candidates, the effect of these particle on structure formation and evolution is expected to be qualitatively different on both large and small scales.

Notwithstanding the difficulties in modeling properly the neutrino particle, several attempts (e.g. Colombi, Dodelson & Widrow 1996; Bode et al. 2001; Macciò et al. 2012; Kamada et al. 2013; Schneider et al. 2013) have been conducted with a successful outcome in solving some of the cases where CDM comes to an impasse. While the methods of CDM simulations have been accurately improved over the last decade, the WDM simulations encounter a number of difficulties in accurately describing the effect of such particles on both large and small scales. In addition to the resolution limitations that are met in the CDM case as well, WDM particles like neutrinos, for example, have a phase space density limit, a Fermi-Dirac distribution and a thermal velocity dispersion. Referring merely to sterile neutrinos, these particles decouple whilst relativistic.

The effects of the initial velocities of the warm dark matter particle are expected to manifest themselves on small scale structure formation. The free streaming exponentially dampens the power spectrum of density fluctuations such that very few structures are formed below the damping scale. Conservation of the fine grained phase space density is expected to set a maximum density that cannot be exceeded during the formation of structures with collisionless particles. For a fermionic WDM particle, we can crudely define the coarse-grained phase-space density $Q \equiv \rho/\sigma^3$, where ρ is the density and σ is the velocity dispersion. This definition is only a good approximation for locally isotropic velocities where the density of particles is not strongly varying.

Different numerical approaches have been used to address the impact of warm dark matter particles thermal velocities. Since the numerical resolution is strongly limited with respect to the physics, one knows that the phase space distribution sampling is anyway poor in space as well as in velocity space. The best compromise is to imprint the physical particle velocity to the simulation particle, as common practice in galactic dynamics. The particle limited sampling is not a sufficient reason to entirely drop the velocity sampling by neglecting the thermal velocities as done in some previous works, while keeping nonetheless the power spectrum cutoff implied by a non-zero thermal velocity (e.g. Schneider et al. 2013; Governato et al. 2015). Nor is the fact that for some dark matter particles the thermal velocities are comparable or smaller than the bulk Zel'dovich velocities. Even though it has been considered difficult to prescribe accurately initial thermal velocities in dark matter simulations, the importance of using them has been emphasized in previous studies like Colombi, Dodelson & Widrow (1996), Bode et al. (2001) and Melott (2007).

In the absence of a tested universal mechanism of production for the warm dark matter particle, the relation between the particle mass and its corresponding thermal veloc-

ity is strongly dependent on the specific model adopted. The widely used formula for generating velocities (Bode et al. 2001) which sets such a relation is based on an assumption that overestimates the number of species at decoupling and in effect underestimates the value of thermal velocities. We will take the opportunity to discuss these assumptions and we will also provide a method for estimating thermal velocities for fermionic, maxwellian and bosonic particles in both relativistic and non-relativistic regimes based on a different set of premises that takes quantum physics into consideration.

Several analyses of warm dark matter simulations in the keV range conclude that the formation of structure is hierarchical, like in cold dark matter simulations. Traditionally, top-down structure formation means forming chronologically the biggest structures first and the smaller ones later, while bottom-up or hierarchical structure formation means the reverse scale order, making it difficult to describe a scenario in which both coexist. In fact it is well known since, e.g., Lin, Mestel, & Shu (1965) and Zel'dovich (1970) that typical structure formation proceeds in time first along pancakes, then filaments and then halos, mixing the large and small spatial scales at all times with different proportions. If we use this terminology in a broader sense, top-down describes the dominant long range effects on structure formation: sheets collapsing into filaments, collapsing into halos. Bottom-up hierarchical structure formation, on the other hand, describes dominant short scale effects, mergers of both early formed and later formed halos. We will examine how both of these mechanisms of structure formation show up in the warm dark matter simulations presented here.

Additional constraints coming from peculiar features may be considered. In cold dark matter models, during the hierarchical evolution caustics are being wrapped inside earlier generations of the merging history, making them invisible in some cases even at high resolutions. However, Cooper et al. (2010) show using cold dark matter simulations that accretion mechanisms of stars and dark matter clumps and disruption of the latter can produce concentric shells that resemble those observed in NGC 7600. In the warm dark matter simulations, as we will see, the shells and caustics are more visible, especially at high redshift, where the top-down formation occurs.

Constraints on the mass of a warm dark matter particle from Lyman- α Forest, cosmic weak lensing, gamma-ray bursts, etc. (e.g. Markovic & Viel 2014; de Souza et al. 2013) give a lower limit in the few keV range. To study the effects of warm dark matter on structure formation, we have, however, explored a larger mass interval, focusing on the region where these effects are more prominent while fairly balanced by the resolution.

The paper is structured as follows: in Section 2 we explain the theoretical reasons for using the thermal component of velocities in the simulations. Subsection 2.2.1 shows how the common used formula for generating velocities in warm dark matter simulations (Bode et al. 2001) is conjectured from hypothetical assumptions. Section 2.2.2 presents a different approach in estimating thermal velocities from the particle mass. In Section 2.3 we discuss some of the inconsistencies found in previous studies. Section 3 describes the parameters used in our simulations while Section 4 shows

the results found from analyzing the simulations. At last, we present our conclusions in Section 5.

2 INITIAL CONDITIONS OF COSMOLOGICAL SIMULATIONS

2.1 Velocities in the initial conditions of cosmological simulations

The initial conditions of most CDM and WDM cosmological simulations have often initial thermal velocity taken as strictly zero, with the argument that at the finite initial redshift the thermal velocity of CDM particles is small in regard of the bulk flow following from Zel'dovich's prescription. We argue below that this practice is numerically inconsistent with the actual problem of describing a collisionless fluid of finite phase space density f . For structure formation, the distribution of the dark matter particles in velocity space is most important, as stressed by Colombi, Dodelson & Widrow (1996).

Indeed, integrating Newton's equation of motion for a set of particles in a force field \mathbf{g} is equivalent to solving in a Lagrangian way with discrete mass particles the collisionless Boltzmann equation with the characteristics method. In conventional notations the Eulerian description of the phase space volume conservation reads,

$$\frac{\partial f}{\partial t} + \mathbf{v} \cdot \frac{\partial f}{\partial \mathbf{x}} + \mathbf{g} \cdot \frac{\partial f}{\partial \mathbf{v}} = 0, \quad (1)$$

where \mathbf{g} is the force field. The mass density ρ is the projection of the phase space density on velocity space:

$$\rho(\mathbf{x}, t) = \int d^3v f(\mathbf{x}, \mathbf{v}, t). \quad (2)$$

The mass density ρ generates the force field \mathbf{g} by Newton's gravity. In a cosmological setup the mean density ρ_0 is subtracted,

$$\begin{aligned} \mathbf{g} &= G \int d^3x' [\rho(\mathbf{x}', t) - \bar{\rho}_0(t)] \frac{\mathbf{x} - \mathbf{x}'}{|\mathbf{x} - \mathbf{x}'|^3} \\ &= G \int d^3x' d^3v [f(\mathbf{x}', \mathbf{v}, t) - \bar{f}_0(\mathbf{v}, t)] \frac{\mathbf{x} - \mathbf{x}'}{|\mathbf{x} - \mathbf{x}'|^3}. \end{aligned} \quad (3)$$

So in this context using vanishing small thermal velocity already poses a consistency problem since f is of the form $\delta(\mathbf{v} - \mathbf{v}_0(\mathbf{x}))\rho(\mathbf{x})$. This implies representing the system with a diverging f in a vanishing fraction of the phase space volume, in other words, mass belongs only to an infinitesimally thin 3D sheet in 6D phase space. As f is conserved along a characteristics, it implies that this singularity must persist at all subsequent times. Methods to conserve arbitrarily high phase space density have been set up (Abel 2012; Hahn & Angulo 2015), but this is not necessarily sufficient. Ideally a physically sound solution f_0 to this Boltzmann-Poisson system should not be numerically sensitive to the initial condition discretization. In practice it is known that the gravitational N -body problem is exponentially sensitive to perturbations (Miller 1964), so the best that can be expected in such simulations is that over an ensemble of simulations with identical statistical initial conditions, results follow a reproducible statistical distribution. Detailed evolution of particles is sensitive to perturbations, but the average evolution of an ensemble of particles is predictable.

When f_0 is finite and differentiable everywhere, in other words when f_0 mathematically exists, the sound situation that should be used, a slight variation of f_0 , a fluctuation, will also follow the same set of equations, so, writing $f = f_0 + f_1$, $\mathbf{g} = \mathbf{g}_0 + \mathbf{g}_1$, where f_1 and \mathbf{g}_1 are the differences between the reference f_0 and the perturbed solution f , and using the fact that f_0 is a solution of the system, we obtain the exact equations for the differences f_1 , and \mathbf{g}_1 :

$$\frac{\partial f_1}{\partial t} + \mathbf{v} \cdot \frac{\partial f_1}{\partial \mathbf{x}} + \mathbf{g}_0 \cdot \frac{\partial f_1}{\partial \mathbf{v}} = -\mathbf{g}_1 \cdot \frac{\partial f_0}{\partial \mathbf{v}} - \mathbf{g}_1 \cdot \frac{\partial f_1}{\partial \mathbf{v}} \quad (4)$$

$$\mathbf{g}_1 = G \int d^3x' d^3v f_1(\mathbf{x}', \mathbf{v}, t) \frac{(\mathbf{x} - \mathbf{x}')}{|\mathbf{x} - \mathbf{x}'|^3} \quad (5)$$

So we see that f_1 follows the same left-hand side equation than f_0 in the unperturbed field \mathbf{g}_0 , except that now the right-hand side contains a source term whose first term $\mathbf{g}_1 \cdot \frac{\partial f_0}{\partial \mathbf{v}}$ is the product of the force fluctuations \mathbf{g}_1 times the gradient of the original f_0 in velocity space. Thus a vanishing zero thermal velocity for a set of particles supposed to represent a physical f_0 is not only suspicious since it corresponds to a delta function in velocity space, but also because the gradient $\frac{\partial f_0}{\partial \mathbf{v}}$ is at least as singular as f_0 . In other words a zero initial thermal width is inconsistent with the initial assumptions, and susceptible to arbitrary strong amplification of perturbations, since the variational equations contain a diverging source term to first order when the initial thermal velocity is small. The only possibility to cancel this diverging term is either to have vanishing force fluctuations \mathbf{g}_1 , which is exceptional when f_1 is non-zero, or that \mathbf{g}_1 is orthogonal to $\frac{\partial f_0}{\partial \mathbf{v}}$, which is also exceptional. The second order term $\mathbf{g}_1 \cdot \frac{\partial f_1}{\partial \mathbf{v}}$ on the right-hand side can cancel the first term only when f_1 is proportional and opposite to f_0 , which is also exceptional. In summary dealing with diverging f_0 is inconsistent with the implicit assumption of regularity of the mathematical problem.

It is instructive to compare how simulating collisionless fluids is differently approached in the fields of stellar and galactic dynamics. While in cosmology the physical collisionless fluids is assumed to consist of elementary particles, in galactic dynamics the fluid is composed of stars. In both cases the numerical simulation particles are order of magnitudes more massive than the physical particles. In the CDM context a simulation particle velocity is seen as representing the bulk flow of a large ensemble of CDM particles, explaining why zero velocity dispersion has been assumed. In galactic dynamics in contrast it is well known that doing so would immediately cause huge gravitational instabilities, and that the correct way to perform collisionless galaxy simulations is to ascribe to the simulation particles the same velocity dispersion as the stars. This is also required for respecting the virial theorem. While the use of velocities has been shown (Melott 2007) to be of importance for the CDM simulations, in WDM it becomes even more relevant (Colombi, Dodelson & Widrow 1996) since the particles do have intrinsic non-zero velocity dispersion. Collisionless fluids are particle mass agnostic, when the particle mass starts to be important is when the 2-body relaxation time is shorter than the system age. Recalling the Chandrasekhar 2-body relaxation time in an arbitrarily large homogeneous medium (Chandrasekhar

1942; Hénon 1973),

$$\tau_{\text{rel}} = \frac{v^3}{8\pi G^2 m \rho \ln N}, \quad (6)$$

where v is the velocity dispersion of N particles of mass m with average density ρ , it is obvious that this relaxation time is proportional to v^3 , $1/m$, and $1/\ln N$, so is exactly zero when $v = 0$. Thus CDM simulations with initial zero v are technically collisional until numerical noise heats the particles to larger v .

From a completely different side of physics, the maximal phase space density constraint set by Heisenberg's inequality,

$$\Delta x \Delta p_x \geq \frac{\hbar}{2} \quad (7)$$

gives a minimum particle velocity dispersion, taking $\Delta x = n^{-1/3}$ and m the particle mass,

$$\Delta v \geq \frac{\hbar}{2} \frac{n^{1/3}}{m} \approx 0.003 \left[\frac{1 \text{ keV}/c^2}{m} \right] \left[\frac{n}{1 \text{ cm}^{-3}} \right]^{1/3} \text{ km/s}. \quad (8)$$

Taking a velocity dispersion lower than this value violates Heisenberg inequality, while taking it only slightly larger means that the particles behaviour is governed by quantum physics, not classical mechanics as assumed in all cosmological N -body simulations.

In summary, adopting even a slight non-zero velocity dispersion in cosmological simulation is certainly a safer and more correct physical assumption than taking strictly cold initial conditions associated with a mathematically singular and inconsistent state leading to situations not under control on the numerical viewpoint due to singular phase space density.

2.2 Thermal velocities of warm dark matter particles

Depending on the WDM particle physics and properties, different scenarios can be considered regarding the particle velocity dispersion as function of redshift. In many scenarios, particles are copiously created in ultra-relativistic conditions and very good thermal equilibrium. As the Universe expands they may subsequently decouple on the thermal point of view because their collisional relaxation rate becomes lower than the expansion rate, while still interacting with the rest of matter by gravitational coupling. If the particles do not decay their comoving number density is conserved, and if they follow the collisionless Boltzmann equation their phase space density is conserved too. But this later assumption is more fragile because some residual elastic collisional relaxation processes can still decrease the effective phase space density by coarse graining.

2.2.1 Inspection of a commonly used result

A frequently cited derivation of WDM particle velocities as function of mass and redshift can be found in Bode et al. (2001). In their Appendix A they recall that for a thermal relict particle X that decouples when relativistic, the abundance n_x relative to photons is:

$$\frac{n_X}{n_\gamma} = \left(\frac{43/4}{g_{\text{dec}}} \right) \left(\frac{4}{11} \right) \frac{g_X}{2} \quad (9)$$

where g_{dec} is the number of relativistic species present at decoupling, and g_X is the number of spin states of the particle. Connecting then the particle mass density $\rho_X = m_X n_X$ with the cosmological parameters $\Omega_X \equiv \rho_X/\rho_c$ and h , where the critical universal density $\rho_c \equiv 3H^2/8\pi G$, and the Hubble constant $H \equiv 100h \text{ km s}^{-1} \text{ kpc}^{-1}$, they derive,

$$\Omega_X h^2 \approx \frac{115}{g_{\text{dec}}} \frac{g_X}{1.5} \frac{m_X}{\text{keV}}. \quad (10)$$

We confirm this equation when using $n_\gamma = 413 \text{ cm}^{-3}$. Then the authors proceed to derive a velocity formula. Since the distribution function of fermions without chemical potential μ is proportional to $(\exp(\epsilon_x/kT_X) + 1)^{-1}$, they point out that if the particles decouple from photons when still relativistic $\epsilon_X = (p_X^2 c^2 + m^2 c^4)^{1/2} - mc^2$ can be replaced by $p_X c$ where p_X is the particle momentum. To keep phase space density constant clearly in the relativistic regime p_X must stay proportional to T_X . But obviously as the regime passes to non-relativistic this argument does not hold, the exact formula valid at all T_X is

$$p_X^2 \propto \left(\frac{kT_X}{c} \right)^2 + 2kT_X. \quad (11)$$

Therefore it seems incorrect to assume that p_X is proportional to T_X also at low T_X . The exact scaling from Eq. (11) becomes $p_X^2 \propto 2kT_X$, or $0.5 m_X v_X^2 \propto kT_X$, that is, the kinetic energy ϵ_X , not the momentum, scales as temperature at all redshifts.

Another problem is the derived constant for velocity. They assume that the distribution function scales as the non-thermal distribution $(\exp(v/v_0) + 1)^{-1}$, and give without detail v_0 (in their Eq. (A3)),

$$\frac{v_0(z)}{1+z} = .012 \left(\frac{\Omega_X}{0.3} \right)^{\frac{1}{3}} \left(\frac{h}{0.65} \right)^{\frac{2}{3}} \left(\frac{1.5}{g_X} \right)^{\frac{1}{3}} \left(\frac{\text{keV}}{m_X} \right)^{\frac{4}{3}} \text{ km s}^{-1} \quad (12)$$

where z is the redshift. But eliminating $\Omega_X h^2$ in this previous equation using Eq. (10) (their Eq. (A2)), we obtain for a $m_X = 1 \text{ keV}$ particle (rounding also to 2 significant digits),

$$\frac{v_0(z)}{1+z} \approx 0.12 \left(\frac{1}{g_{\text{dec}}} \right)^{1/3} \frac{\text{keV}}{m_X} \text{ km s}^{-1}. \quad (13)$$

Thus we find $g_{\text{dec}} = 1000 (g_X/1.5)^{1/3}$. This is too high a value for g_{dec} to be endorsed, as mentioned by the authors, by large entropy producing processes. Since the value for g_{dec} varies linearly with the mass of the particle in the given cosmological model (Eq. 10), it allows the elimination of g_{dec} from the final expression for velocity¹. This high value used for g_{dec} leads to a significant decrease in the particle velocities, as shown in Table 1.

In the minimal standard model the number of the full set of particles is ~ 107 while in the minimal supersymmetric standard model, the value is increased to ~ 229 (Pierpaoli et al. 1998). Previous studies like Colombi, Dodelson &

¹ The authors cite a value of 688 for the number of relativistic degrees of freedom at the time of decoupling of a 1 keV particle, while then using the value of 1000. In Viel et al. 2005 this latter value is used, although a rigorous calculation gives 903 as the exact value.

Widrow (1996)² use a value of ~ 100 for right-handed neutrinos decoupling before the electroweak phase transition at very high temperatures, while Pierpaoli et al. (1998) assume a conservative reference value of 150 for both gravitino and a standard warm dark matter candidate like the massive neutrino.

The lower value for the velocity adopted by Bode et al. (2001) has been used in most WDM simulations thereafter. This value for g_{dec} , however, is valid for a 1 keV particle only if we assume that dark matter is made entirely by these type of particles, as shown in Eq. (10). For the cases in which a certain warm dark matter particle represents only a fraction of the total dark matter content, this value is different and Eq. (12) needs to be scaled accordingly. This aspect has been overlooked in some simulation studies of mixed dark matter, providing misleading results as we will show in Section 2.3.

The next line following Bode et al. (2001) Eq. (A3) states: “The rms velocity is $3.571v_0$ ”. Recalculating the rms velocity of the adopted distribution function $f = (e^{v/v_0} + 1)^{-1}$ we find a slightly larger factor:

$$\langle v^2 \rangle = \frac{\int_0^\infty 4\pi v^4 f dv}{\int_0^\infty 4\pi v^2 f dv} = 15 \frac{\zeta(5)}{\zeta(3)} v_0^2 \approx (3.59714v_0)^2, \quad (14)$$

where ζ is Riemann’s function. The slight discrepancy (the 9 digit) appears thus as a misprint.

In Appendix A we find that the largest correction factor for the rms speed of a Fermi-Dirac distribution with respect to a Maxwellian distribution is 1.07, not ≈ 3.6 as stated in Macciò et al. (2012). The difference comes entirely from the very non-thermal distribution.

2.2.2 Another scenario for quantum semi-degenerate particles

In the previous Bode et al. (2001) scenario, WDM particles are treated as localized mass bullets following Boltzmann’s equation. However, at creation time they are also assumed to be ultra-relativistic and in thermal equilibrium with radiation and the rest of matter, typically following a Fermi-Dirac distribution since the known stable particles are fermions. This entails that their quantum nature does play a role at birth, they are at least semi-degenerate. Phase space density is high enough for the distinction between classical and quantum particles to play a role. The non-local Pauli principle applies then, each particle “knows” about the state of each other. Now if phase space density is approximately conserved then particles remain semi-degenerate at all times, which is inconsistent with the usual assumptions applied at low redshifts that they behave as classical particles.

The known neutrinos offer a good example that particles are quantum objects instead of localized mass objects. Real neutrinos are in addition of being fermions also in a superposition of three mass states. Since mass states propagate at different velocities, with time relict neutrinos are actually in a superposition of entangled mass states increasingly spread apart. How gravitational interaction with matter structures can destroy the coherence of these entangled

states is a question that will need to be addressed in future works.

Here we develop a procedure to calculate precisely the particle velocity valid in all relativistic regimes for fermions or bosons. The full distribution Fermi-Dirac or Bose-Einstein distribution reads (e.g., Padmanabhan 2002)

$$f(\mathbf{p}) = \frac{g}{(2\pi\hbar)^3} \frac{1}{\exp((\epsilon - \mu)/kT) \pm 1}, \quad (15)$$

where \mathbf{p} is the particle momentum, g the spin-degeneracy factor (of order 1 or 2), μ the chemical potential, $\epsilon = \sqrt{p^2 c^2 + m^2 c^4} - mc^2$ the particle energy, m the particle mass, and T the particle temperature. The comoving number density is calibrated according to a neutrino-like scenario where the particles are once coupled to the photon background and in thermal contact, at a time where gravitational perturbations are still linear.

First, the assumption that the chemical potential μ is constant and negligible is not necessarily valid for identical fermions which are created in a half-degenerate state. The Pauli principle has for effect that identical fermions, even with negligible interaction (like the weak nuclear force for neutrinos), possess an effective *exchange potential*, also sometimes called *exchange-correlation potential* (e.g., Atkins & Friedman 2005). In quantum chemistry and Density Functional Theory (DFT) the exchange potential is well known to be essential in the Hamiltonian describing electrons around a nucleus, or electrons in materials, although the exact form in different contexts is sometimes not well known. In the cosmological context the exchange potential changes the chemical potential as the spatial density of identical fermions changes. This effective repulsive interaction for fermions makes the collisionless assumption of free fermions much less obvious. In Pfnigiger & Muccione (2006) the effective interaction of free fermions was illustrated by solving exactly the time-dependent Schrödinger equation for two free but identical fermions in 3D space starting as Gaussian wave packets. In the quantum regime (high phase space density) these wave packets effectively interact and are scattered due to the repulsive exchange potential. In the classical regime (low phase space density) the wave-packets follow, as expected, a straight trajectory.

In quantum statistical mechanics (Huang 1987) the exchange potential between two particles has a well known form dependent on temperature and distance r

$$\phi(r) = -kT \log \left(1 \mp \exp \left(-mkT \frac{r^2}{\hbar^2} \right) \right) \quad (16)$$

$$= -kT \log \left(1 \mp \exp \left(-2\pi \frac{r^2}{\lambda^2} \right) \right), \quad (17)$$

where the $-$ sign applies for fermions and $+$ for bosons, and λ is de Broglie wavelength. For semi-degenerate particles λ is of order of $n^{-1/3}$, so in a semi-classical description fermions “feel” a rapidly varying repulsive force from neighbouring particles, while bosons an attractive force. The reality of the exchange potential can be invoked to cast a doubt that the commonly assumed collisionless approximation for semi-degenerate particles is valid in the cosmological context. Instead one should expect a local thermalization of identical particles on a short time-scale.

To calculate the chemical potential evolution in the cosmological context, one needs therefore an additional assumption

² Interestingly this is the paper cited by Bode et al. (2001) as reference for production mechanisms of WDM and their relation to cosmology

tion, besides number conservation. The particle momentum and kinetic energy can not be assumed conserved due to the global gravitational interaction. A reasonable assumption (Trodden & Carroll 2004) is that the expanding medium proceeds adiabatically, at least as long as gravitational clustering is linear. This means that the particle specific entropy can be taken as a conserved quantity.

The entropy S expressed as a function of other thermodynamical variables reads (e.g., Padmanabhan 2002, Vol. I, Eq. 5.73),

$$S = \frac{1}{T} (E + PV - \mu N) , \quad (18)$$

where E is the total thermal energy, P the pressure, V the volume, μ the chemical potential, and N the number of particles. The specific entropy $s \equiv S/N$ divided by Boltzmann's constant k is a pure number

$$\frac{s(T, \mu)}{k} = \frac{1}{kT} \left(\frac{e + P}{n} - \mu \right) \quad (19)$$

where $e = E/V$ is the specific energy density and $n = N/V$ is the number density.

The thermodynamical quantities for fermions and bosons at all regimes can be calculated accurately by evaluating numerically the relativistic Fermi-Dirac or Bose-Einstein integrals for particle density n , energy density e , and pressure P (e.g., Padmanabhan 2002, Vol. II, p. 216) as functions of temperature T and chemical potential μ ³:

$$n(T, \mu) = \frac{4\pi g}{h^3} \int_0^\infty \frac{p^2}{\exp((\epsilon - \mu)/kT) \pm 1} dp , \quad (20)$$

$$e(T, \mu) = \frac{4\pi g}{h^3} \int_0^\infty \frac{p^2 \epsilon}{\exp((\epsilon - \mu)/kT) \pm 1} dp , \quad (21)$$

$$P(T, \mu) = \frac{4\pi g}{h^3} \int_0^\infty \frac{p^2}{\exp((\epsilon - \mu)/kT) \pm 1} \frac{1}{3} \frac{c^2 p^2}{\epsilon + mc^2} dp , \quad (22)$$

where g is the number of distinct particle states, and $\epsilon = \sqrt{p^2 c^2 + m^2 c^4} - mc^2$ the particle energy. In the integrands the $+$ sign is for fermions, the $-$ sign for bosons. The conserved particle density $n(T, \mu)$ is related to universal expansion by the scale factor $a = 1/(1+z)$, thus

$$n(T(z), \mu(z)) = n_0 (1+z)^3 , \quad (23)$$

while the constant particle entropy gives

$$\frac{s(T(z), \mu(z))}{k} = \frac{s(\infty, 0)}{k} = 4.20183245 , \quad (24)$$

For Fermi-Dirac particles the solution of this system for $n_0 = 115 \text{ cm}^{-3}$, $m = 1 \text{ keV}$, $g = 1$ in the non-relativistic regime is :

$$\frac{\mu}{kT} = -1.6202, \quad \frac{mc^2}{kT} = 5.6186 \cdot 10^{12} . \quad (25)$$

For a graphical illustration of these functions behaviour, see

³ This part follows closely the calculations made in Pfnigiger & Muccione (2006), but correct a mistake where the used entropy expression was only valid in the ultra-relativistic regime, or when $\mu = 0$.

Fig.B1 in Appendix B. For a couple of dex around this solution the scaling with n , g and m for T and v goes with good approximation as follow⁴:

$$\begin{aligned} T &= 2.0654 \cdot 10^{-6} \left(\frac{n}{115 \text{ cm}^{-3}} \frac{1}{g} \right)^{2/3} \left(\frac{mc^2}{\text{keV}} \right)^{-1} \text{ K} \\ v &= 0.2226 \left(\frac{n}{115 \text{ cm}^{-3}} \frac{1}{g} \right)^{1/3} \left(\frac{mc^2}{\text{keV}} \right)^{-1} \text{ km s}^{-1} . \end{aligned} \quad (26)$$

When the regime becomes relativistic this approximation is no longer accurate. One can solve the pair of equations (23) and (24) in any situation.

In comparison, for Bose-Einstein particles the solution for the same parameters is:

$$\frac{\mu}{kT} = -1.2451, \quad \frac{mc^2}{kT} = 8.1348 \cdot 10^{12} . \quad (27)$$

Around this solution the scaling with n , g and m for T and v goes approximately as:

$$\begin{aligned} T &= 1.4265 \cdot 10^{-6} \left(\frac{n}{115 \text{ cm}^{-3}} \frac{1}{g} \right)^{2/3} \left(\frac{mc^2}{\text{keV}} \right)^{-1} \text{ K} \\ v &= 0.1768 \left(\frac{n}{115 \text{ cm}^{-3}} \frac{1}{g} \right)^{1/3} \left(\frac{mc^2}{\text{keV}} \right)^{-1} \text{ km s}^{-1} . \end{aligned} \quad (28)$$

If Maxwell-Boltzmann particles are used in simulations one can also calculate the solution, replacing the ± 1 in integrals by zero, and taking $s(\infty, 0)/k = 4$. The velocity coefficient is found to be $0.20592 \text{ km s}^{-1}$, intermediate between the Fermi-Dirac and Bose-Einstein cases. The correction of quantum statistics with respect to a Maxwellian distribution remains thus small, as demonstrated in Appendix A.

2.3 Power spectrum of the warm dark matter simulations

Since collisionless physics does not depend on the particle mass, the power spectrum must directly depend only on the velocity distribution of the particles, which results from the particle production mechanism. Colombi, Dodelson & Widrow (1996) and Bode et al. (2001) also emphasize this point.

To compute the transfer function for WDM models the fitting formula suggested by Bode, Turok and Ostriker (2001) gives:

$$T^2(k) = \frac{P^{\text{WDM}}}{P^{\text{CDM}}} = [1 + (\alpha k)^{2\nu}]^{-10/\nu} \quad (29)$$

where α , the scale of the break, is a function of the WDM parameters, which are function of the velocity, while the index ν is fixed. People prefer however, to use the mass dependence instead of the velocity, using Eq. (13) as a conversion.

⁴ An astute reader might notice that for classical massive neutrinos ($0.01 < mc^2/\text{eV} < 2$) the found temperature is much lower than the commonly quoted temperature of 1.9 K. Actually the 1.9 K value is valid for massless neutrinos only. The difference comes from the misleading use of temperature as an equivalent concept for energy and vice versa, while the neutrino rest mass energy does not contribute to thermal energy. The proper meaning of temperature is the quantity that would be measured, in the case of real neutrinos, by a cosmic sized thermometer able to thermalize with the neutrino background.

Viel et al. (2005) (see also Hansen et al. (2002)), using a Boltzmann code simulation, found that $\nu = 1.12$ is the best fit for $k < 5 h \text{ Mpc}^{-1}$, and they obtained the following expression for α :

$$\alpha = 0.049 \left(\frac{m_x}{1 \text{ keV}} \right)^{-1.11} \left(\frac{\Omega_\nu}{0.25} \right)^{0.11} \left(\frac{h}{0.7} \right)^{1.22} h^{-1} \text{ Mpc}. \quad (30)$$

In the case of warm dark matter particles, the streaming velocity suppresses the matter power spectrum $P(k)$ and the formation of structure, on scales smaller than their free-streaming scale. A rough estimation of the free-streaming scale is given by Bond et al. (1980):

$$k_{\text{FS}} = \frac{2\pi}{\lambda_{\text{FS}}} \sim 5 \text{ Mpc}^{-1} \left(\frac{m_x}{1 \text{ keV}} \right) \left(\frac{T_\nu}{T_x} \right), \quad (31)$$

Depending on the model for the properties of a certain particle, there can be different expressions for the damping of the power spectrum (Abazajian & Koushiappas 2006, e.g.), but for the purpose of our present work and for easier comparison with previous studies we use the expression given in Eq. (30) with the corresponding thermal velocities.

This approach used for cutting the power spectrum is only valid however, for a scenario in which the whole dark matter content is made up by one specific dark matter particle of a certain velocity.

2.4 Caveat Emptor

In this section we would like to summarize the findings of previous sections and discuss some of their implications. We want to stress that the assumed particle production model and physics strongly impact on the ascribed particle mass, while the initial velocity distribution and its corresponding power spectrum is the only really important initial parameter influencing the simulation results. As far as the physics behind the origins of the dark matter particles is concerned, the assumptions found in the literature can widely differ.

Previously on section 2.2.1. we showed how the Bode et al. (2001) result for estimating velocities for neutrino like particles is based on arguments like entropy production and negligible chemical potential. The expression for velocities in Eq. (12) is based on a dependence of the number of species on the mass of the particle, such as to preserve the equivalence in Eq. (10). For the models with cold plus warm dark matter, or models with different particle mass, the value of the number of species should be adjusted accordingly. Many papers that study mixed particles simulations have omitted this readjustment for velocities (e.g. Anderhalden et al. 2012). Eq. (12) has been reduced by the fraction with which a certain particle contributes to the total density, therefore leading to inconsistencies like having for a certain mass of a particle, different thermal velocities, depending solely on that fraction. Moreover, since the power spectrum cutoff depends on the velocity of the particle (not the mass), studies that use the cutoff for a velocity, but a different thermal velocity, given by a different model of particle production are not consistent. These results, although used for constraining the mass of a particle in terms of detection experiments, should not be considered as accurate.

As an alternative, we provide a different energy-thermal velocity correspondence based on number conservation and a

Table 1. Correspondence between particle mass m and rms velocity dispersion in literature for 0.2, 1 and 3.5 keV. The first column shows the value originally given in Bode et al. (2001), the second column shows the value obtained using $g_{\text{dec}} = 150$ (Pierpaoli et al. 1998) in Eq. (12), and the third one, the value given by our derivation.

Mass	Bode et al. Eq. (11) $\times 3.571$	Pierpaoli et al. km/s	This work Eq. (25) km/s
keV/ c^2	km/s	km/s	km/s
0.2	0.366	0.4032	1.113
1.0	0.0429	0.0225	0.223
3.5	0.00806	0.0230	0.0636

non-entropy production while taking into account the quantum pressure, but assuming a thermalization caused by the exchange potential. Entropy conservation by particles in the hot Big Bang is invoked by many authors, such as Padmanabhan (2002) or Weinberg (2008). From Eq. (26) which estimates the thermal speed of WDM particles, independent of the cosmological parameters, we have the following velocity dependence with the redshift:

$$\frac{v}{1+z} = 0.2226 \left(\frac{n}{115 \text{ cm}^{-3}} \frac{1}{g} \right)^{1/3} \left(\frac{mc^2}{\text{keV}} \right)^{-1} \text{ km s}^{-1}. \quad (32)$$

The difference between our and Bode et al. (2001) estimations is showed in Table. (1) for 0.2, 1 and 3.5 keV respectively, at redshift zero. The Bode et al. (2001) speed for 1 keV fermions out of equilibrium, used in most WDM simulations, is 5 times lower than the value derived here. In general these differences cumulate their effect if simulations are started at higher redshifts, and are crucial not only for phase space density studies, but also for structure formation.

Our finding affects the results and conclusions of previous papers which were using Eq. (12) to constrain the mass of sterile neutrinos. This extends even to papers which did not include thermal velocities. The power spectrum studies based on the velocity of the particle are subject to the same difference in the velocity estimation (see Section 2.3). Also, when comparing the thermal velocities to the Zeldovich velocities, these factors weaken correspondingly the reason for ignoring the thermal velocities, against all the arguments presented in Section 2.1.

Since our aim here is to describe typical qualitative effects on structure formation present in a broader range of energies, we will refer to the particles in terms of their velocity dispersion instead of their mass. Indeed the thermal velocity of a particle as its decoupling temperature at a certain redshift depends on the specific physics of particle production. That influences the ascribed mass of that particle. More complex analysis of the decoupling theories for a certain particle may give a slightly different dependence between the thermal velocity at a certain redshift and the particle mass.

3 SIMULATIONS SETUP

We conducted several suites of N -body simulations. All simulations have been performed once with PKDGRAV-2, a treecode written by Joachim Stadel and Thomas Quinn

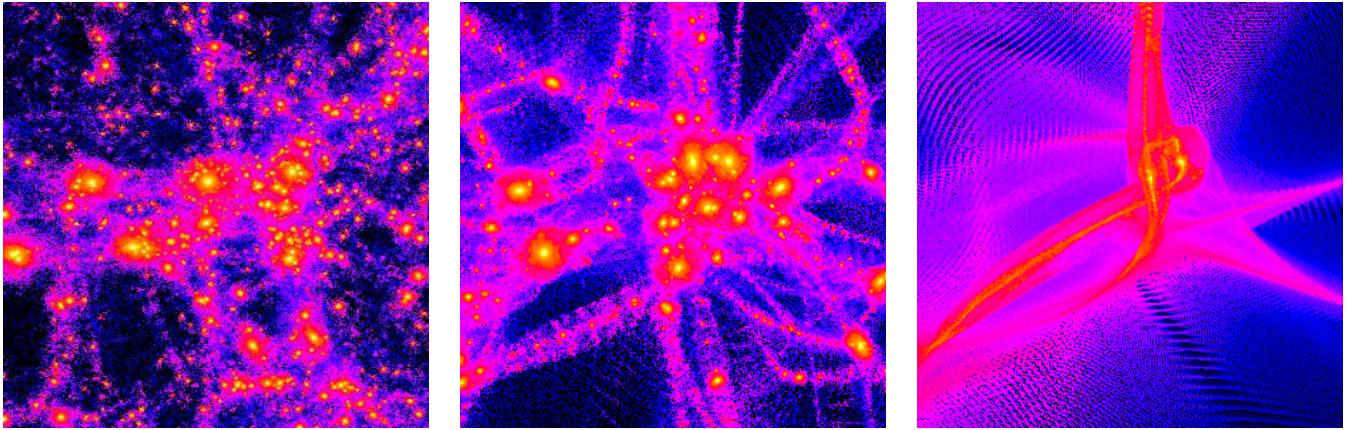


Figure 1. Illustrative density map of structure formation regions at redshift zero, from left to right, in CDM, WDM (0.3 km/s) and HDM (2.3 km/s). For a similar illustration of a full box see Macciò et al (2012). These simulations have not been used in this paper.

Table 2. Details of the simulations

Label	velocities z_i km/s	cutoff eV	box size Mpc/h	N	softening pc
CDM	no	-	40	300^3	50
WDM1	no	200	40	300^3	50
WDM2	36.6	200	40	300^3	50
WDM3	no	1000	40	300^3	50
WDM4	4.6	1000	40	300^3	50
WDM5	36.6	200	30	256^3	100

(Stadel 2001)⁵ and then using Volker Springel’s Gadget-2 (Springel 2005)⁶. The initial conditions are generated with Ed Bertschinger’s GRAFIC2 package (Bertschinger 2001)⁷. Although some differences have been spotted between the two different codes, those differences are not qualitatively important where structure formation is concerned, there can be minimally spotted at very small scales.

The simulations we have performed cover a range of velocities from 0.01 km/s to 10 km/s (3.5 keV to 15 eV) at redshift zero. For illustration purposes, in Fig. 1 we show generic density maps of structure formation regions in CDM, WDM and HDM simulations. Particles that have ~ 0.1 km/s velocity dispersion are in a transient regime from a predominant top-down structure formation scenario to a hierarchical one, showing both these trends. We have chosen one such simulation and compared it to a simulation of a colder particle more favored by the observational constraints and with a cold dark matter simulation. For the warm dark matter the simulations have been prepared with initial power spectrum consistent with initial velocities, and, for comparison, the same initial power spectrum without initial velocities.

The simulation parameters are summarised in Table 2. The starting redshift for the simulations is $z_i = 100$ in order to ensure a proper treatment of the non-linear growth of cosmic structures.

The cosmological parameters used are given by the

WMAP7 results: $\Omega_\Lambda=0.721$, $\Omega_m=0.279$, $\Omega_b=0.0463$, $h = 0.7$ and $\sigma_8 = 0.821$,

We start with running large scale simulations in cosmological box of 40 Mpc/h, engaging 300^3 dark matter particles and one 30 Mpc/h box with 256^3 particles. We then select a region where the top-down halo formation is predominant and re-simulate it with an eight times higher resolution.

4 SIMULATIONS ANALYSIS AND RESULTS

4.1 Structure formation in WDM simulations

Free streaming causes a delay in the formation of structure in the warm dark matter simulations. This delay depends on the energy, hence the velocity of the particle. The higher the thermal velocity of the particle, the later the filaments will reach the collapse, making it impossible for structures to be formed by redshift zero in hot dark matter scenarios, as illustrated in Fig. 1, right panel.

The fragmentation of the filaments is observed in all N-body simulations of warm dark matter where the collapse is stimulated by the noise in the particle distribution (Bode et al. 2001; Götz & Sommer-Larsen 2002; Wang & White 2007). This is especially observable at the characteristic grid or glass spacing. Above the free streaming scale the mass function is flattened to a value that closely matches the luminosity function of galaxies (assuming mass traces light). The length and the lifetime of the filaments depend on the energy of the particle. The higher the velocity dispersion of the particle, the larger will be the filaments and the longer they will be preserved. These can reach 20 Mpc in a 40 Mpc box and survive until redshift zero in the case of velocities of few km/s and above.

In Fig. 2 the difference between high density regions in a CDM simulation, versus WDM at redshift 2.3 is shown. The picture displays the 2D projection of the 3D density map of the full simulation box. One can see that due to the free streaming, particles are concentrated in large spatial structures, delimited from each other by large low density regions, or voids, as opposed to the crowded web present in the cold dark matter simulation.

It is well known that in CDM models, smaller halos

⁵ <http://hpcforge.org/projects/pkdgrav2/>

⁶ <http://www.mpa-garching.mpg.de/gadget/>

⁷ <http://web.mit.edu/~edbert/>

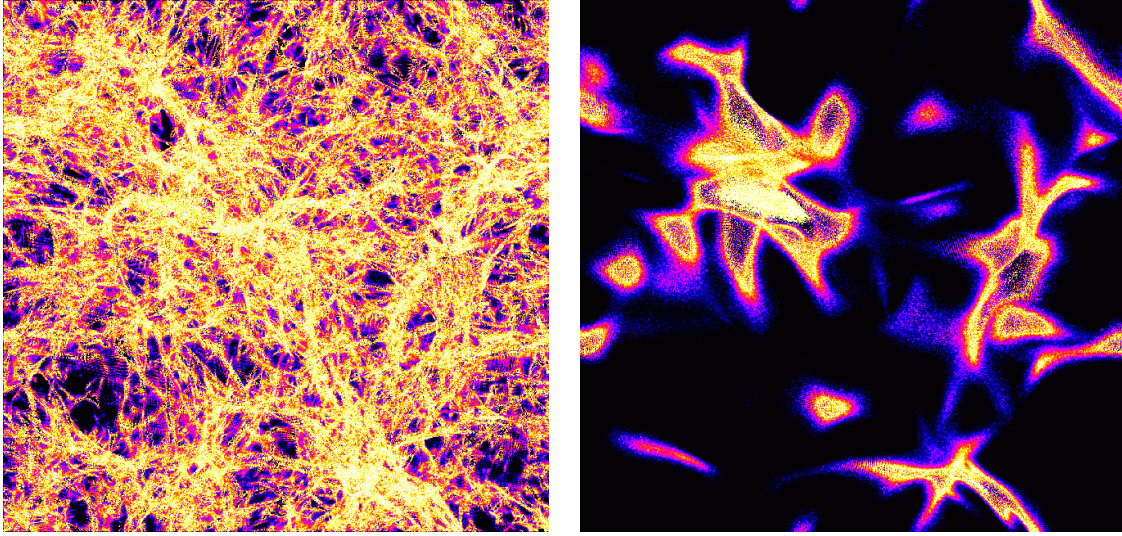


Figure 2. Plot of high density regions at redshift 2.3 in a 40 Mpc/h simulation box with CDM particles in the left panel and WDM particles (model WDM2) in the right one, showing major topological differences

collapse first and merge hierarchically into larger systems, as it is obvious in all high resolution simulations (Diemand & Moore 2010, 2011; Stadel et al. 2009). Furthermore, one finds that less massive halos are more concentrated, perhaps reflecting the fact that the density of the universe is higher at earlier epochs, since the CDM particles have an infinite phase space density.

On the other end of the velocities spectrum, for HDM models, the structure formation is essentially top-down up to redshift zero, as can be seen in the right panel of Fig. 1, with just large filaments collapsing into few halos.

As stated in the introduction, in the case of warm dark matter we see from our simulations that the structure formation is more complex, a hybrid mechanism where both long-range and short-range effects are present, from long distance to nearest neighbours, from top-down to bottom-up.

The top-down trend predominant in the early epochs in warm dark matter simulations has been missed in previous works since it is difficult to observe it while analyzing the snapshots of the simulations. For particles with velocities smaller than a few km/s the top-down trend is hidden by the hierarchical growth that dominates at later times. We have been able to see this effect in our simulations while watching movies made with a sufficient large number of snapshots. We stress that only movies convey the complexity of these multiscale hierarchical processes. Several movies of WDM structure formation, filament collapse and halo formation from this study can be found on a youtube playlist (<https://www.youtube.com/playlist?list=PLnGS4wkStJ1aqi3M9hTDaUzuZ-vs-Qg6i>)⁸.

As the movies show, in WDM simulations, structures form in a qualitatively different way from CDM models. The

hybrid structure formation is more complex than what the traditional top-down/bottom-up dichotomy can categorize, as discussed in the Introduction.

- During the early stages one sees the formation of well contoured filaments. How early is this stage depends on the particle velocity. In our WDM2 simulations this happens in the interval $13 > z > 8$.
- In the higher density regions, usually situated at the intersection of such filaments, the first halos are formed through gravitational collapse. These halos continue growing into larger ones by accreting particles from the disrupted filaments (Fig. C1).
- In medium density regions, halos show a hierarchical formation trend. Small halos collapse first and then merge into bigger halos (Fig. C2).
- In less dense regions, the ones isolated by voids and which have a very slow evolution, we have observed filaments that collapse very late. The top down formed halo survives without any mergers until redshift zero (Fig. C3).
- Finally there is the more complex scenario in which we observe large halos formed earlier which merge together forming a large cluster (Fig. C4).
- The filamentary-like structure is preserved until redshift zero, with new filaments forming in the low density regions as late as redshift $z \sim 4$.

Looking closer, we have analyzed four different regions in our simulations and displayed them in four different movies. The characteristics of these regions are summarized in Table 3.

Our conclusion from analyzing these simulations is that there is only one correlation, between the time of the first collapse and the density reached in a certain region, and that depends only on the network morphology and architecture of that region. The first halos collapse in the region where the density becomes $\sim 2 \times 10^3$ times larger than the average density and almost $\sim 3 \times 10^3$ times larger than the lowest densities present in that region at that epoch. In the simulations with particle velocity of 0.36 km/s (that mimic

⁸ All the HD movies are on youtube and can be watched individually on this channel <https://www.youtube.com/channel/UCeMQi8hDNW2emqGn-urtvpg>. Remember to adjust your settings to HD quality. Links for direct download can be provided on demand. For a short description of the movies and movies snapshots, see Appendix C.

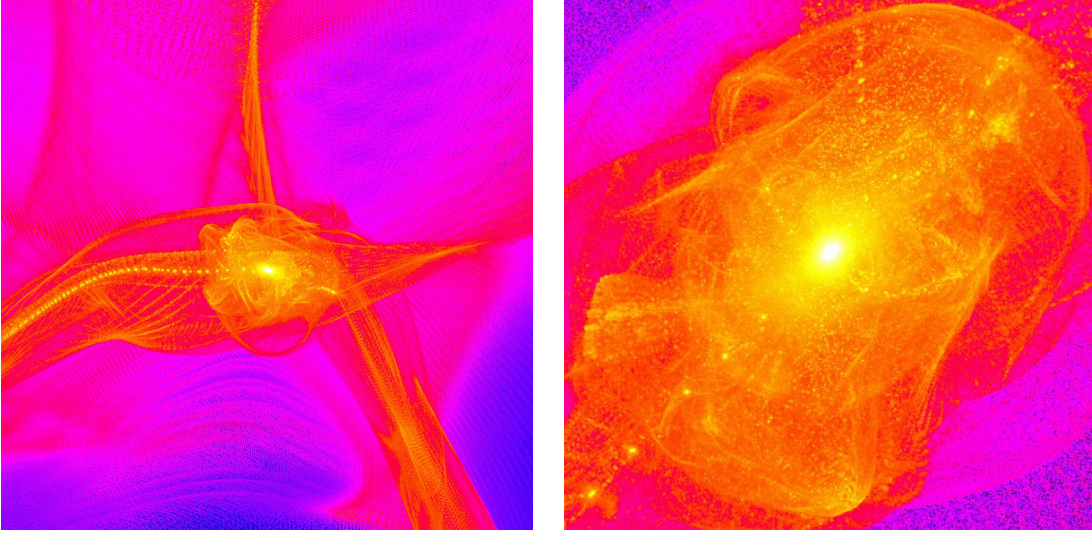


Figure 3. Halo formation at the intersection of filaments. A zoom in projection shows that shells and caustics are visible in the not yet virialized WDM halo.

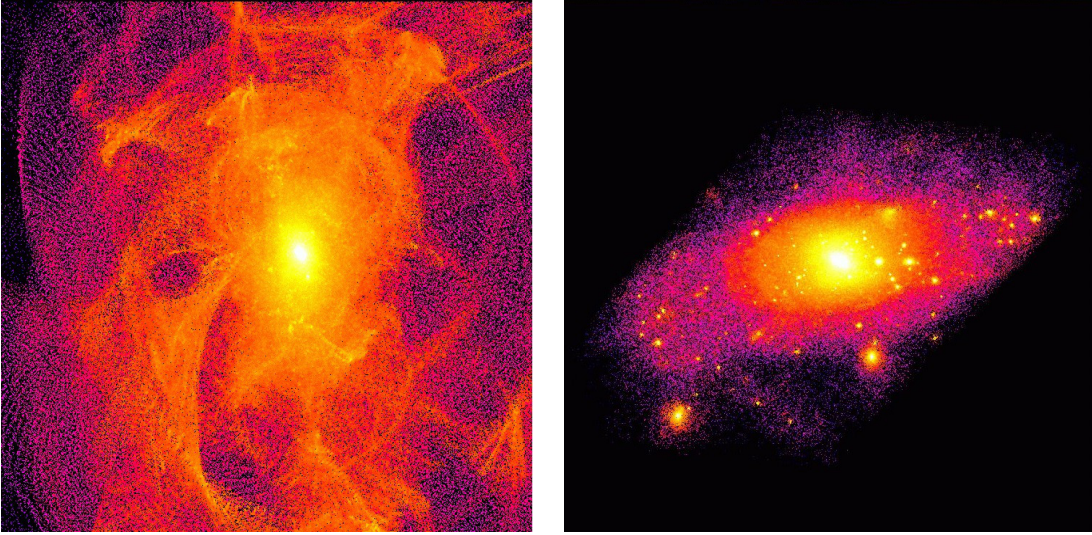


Figure 4. A thin slice of the WDM halo formed Top-Down on the left and of a CDM one on the right. Very different internal structure, with shells in caustics in the WDM halo being more apparent

Table 3. The properties of four different regions of simulation WDM2 displayed in the movies

Label	size	first collapse	average density	highest density
-	box	z	critical	critical
lu.avi	1/4	10.13	0.264	477
ld.avi	1/4	9.45	0.258	481
ru.avi	1/4	10.77	0.268	480
rd.avi	1/4	9.78	0.258	474

200 eV), the first collapse appears just after redshift 10 with the first halos forming until redshift 4, while in the simulations with 0.04 km/s (that mimic 1 keV), the first structures would have been already formed by redshift 10. The first halos form at the high density region at the intersection of the

filaments and then continue accreting matter. If in a certain region there are many filaments collapsing, then the halos will merge into bigger ones.

Due to the free streaming velocity of the particles, the network configuration and architecture of a certain region is rapidly changing. When the density becomes higher in more isolated regions, the collapse occurs even later, after redshift 4 and some of those halos do not suffer mergers (Fig. C3), so there are halos at redshift zero that have formed via a top-down scenario and did not grow through hierarchical mergers. This is an interesting result, since the observations show that a large fraction of halos in the universe have not suffered any mergers until redshift zero.

Why a certain region has more a top-down or bottom-up formation history depends only on the spatial distribution of the filaments in a certain simulation.

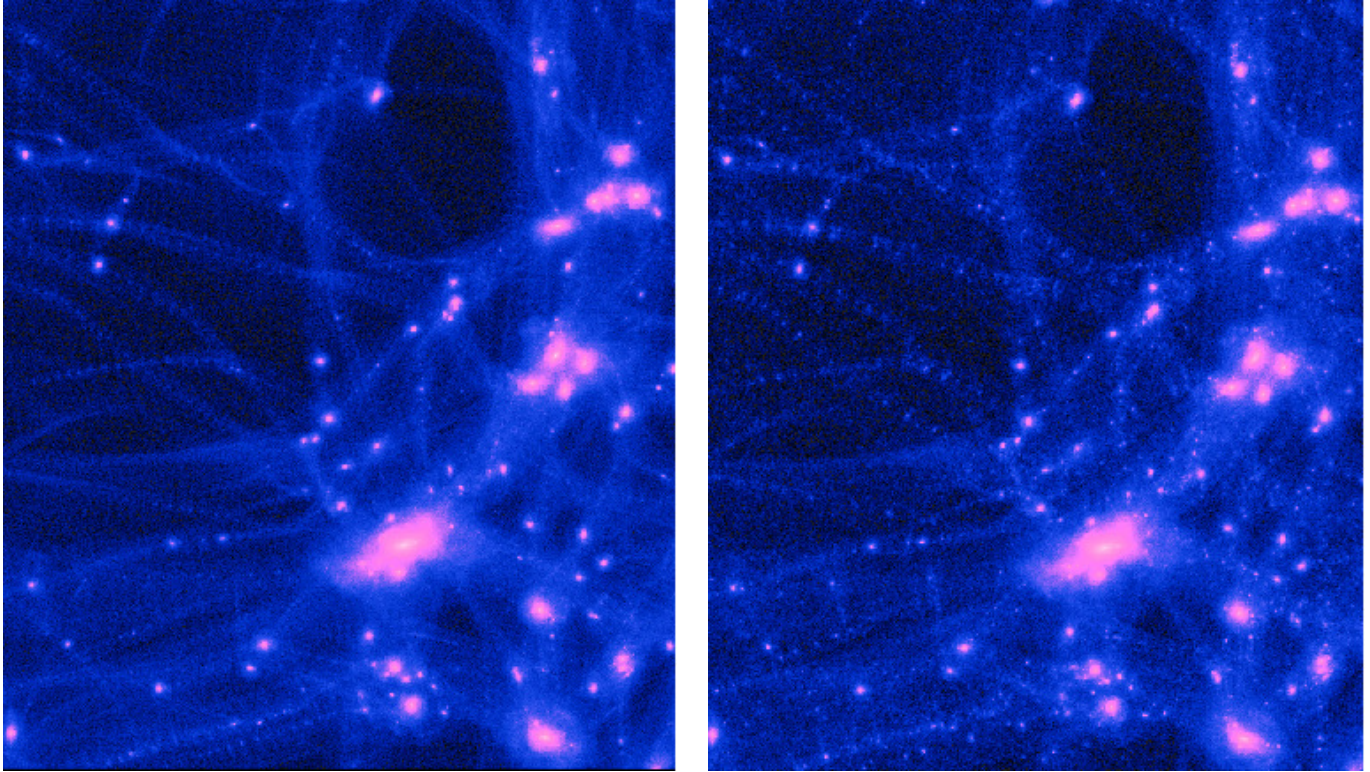


Figure 5. A zoom in simulations with the same cutoff in the power spectrum having corresponding thermal velocities - WDM2(left) and no thermal velocities WDM1(right) at $z=0$

A single halo simulated with different velocities can be seen in the movie `halo.avi`⁹. The $7 \times 10^{12} M_{\odot}$ halo forms top-down at the intersection of the filaments and has 18 million particles in its r_{200} radius.

These high resolution runs are 8^3 times more resolved in mass than the initial ones: the dark matter particle mass is $m_d = 2.72 \times 10^5 M_{\odot}$, where each dark matter particle has a spline gravitation softening of 355 pc.

Although the WDM halos on galactic scales contain few bound substructures, one can see shells and caustics inside the virialized region which arise from the coherent infall of material along filaments and from the smooth surrounding regions. As the resolution increases, the presence of shells and caustics becomes more apparent. The early top-down formation of a halo at the intersection filaments is shown in Fig. 3 along with a zoom in its central region. One can clearly see the shells and caustics wrapped inside the 18 million particle halo. A thin slice projection of the warm dark matter halo and a cold dark matter one, clearly illustrates in Fig. 4 how strikingly different is their inner structure.

4.2 Impact of thermal velocities on structure formation

As stressed in Section 2, the use of thermal velocities in warm dark matter simulations is crucial, even if their value

is comparable with the Zeldovich velocities at a certain redshift.

In Fig. 5 we show the differences at redshift zero between the structures emerging in a region in two similar simulations, WDM1 (without thermal velocities), and WDM2 (with thermal velocities). Both simulations have the same size, the same power spectrum cutoff and the same initial redshift. The structure formation and evolution in these two simulations is shown side by side in movie `cosmoboxall.avi`¹⁰.

We can see that although the position of the big structures is not affected, below Mpc scales there is a memory of the grid in the simulation without velocities that is smoothed out when adding thermal velocities, as expected. Some of the very small halos formed in the simulation without velocities cannot be found in the simulation where thermal velocities are included. The lack of small halos in WDM simulations with velocities is of course a crucial feature hinting to resolve the discrepancy between the CDM simulations predicting too many subhalos in galaxy-sized halos in comparison with the observed number of dwarf galaxies around large galaxies. Indeed WDM simulations without velocities still suffer from the infinite phase space density problem.

For comparison, we have performed a suit of simulations that start with a cold distribution of particles, no power spectrum cutoff, but have velocities corresponding to 1 km/s, 10 km/s, 200 km/s and 700 km/s. Even the early structure formation is qualitatively different from the warm

⁹ The movie can be found on youtube https://www.youtube.com/watch?v=s_H4dSOP27I. A zoom in the halo can be watched at <https://www.youtube.com/watch?v=zqVi9SSWmXM>

¹⁰ The movie can be watched here: <https://www.youtube.com/watch?v=5txGwBRNC1U>

dark matter simulations, confirming that the top-down collapse is induced by the damping of the power spectrum at small scales and not the thermal velocities.

4.3 Technical aspects in simulating WDM

The resolution limit poses even a more stringent problem in warm dark matter simulations than in cold dark matter ones. Indeed, in order to properly analyze a region of the simulation, multiple refinements of that region with higher resolution particles are used. This implies tracking the particle backwards, from redshift zero to the initial conditions. Due to the large streaming velocities, particles that end up in a virialized halo at redshift zero come from a larger region than in the CDM simulations, making it more difficult to reach high resolution simulations in WDM.

The heavier the effective mass of our simulation particles, the more prominent is the 2-body relaxation effect in small clumps (Eq. (6)). This problem is more stringent in the case of cold dark matter simulations, where an initial zero velocity is used. In the case of warm dark matter, this scales with the velocity of the particle, giving a smaller relaxation time for a smaller velocity. This is why for simulations in the keV range, where the streaming velocity is smaller, the top-down formation history has been barely observed.

As recently shown by Gao, Theuns & Springel (2015), methods like ‘FoF’ used in analyzing cold dark matter simulations are proved to be insufficient in analyzing warm dark matter halos. We confirm this statement, finding that the artificial fragmentation occurring along the filaments results in a high number of small halos with less than ten particles.

5 CONCLUSIONS AND DISCUSSION

We have performed several N-body warm dark matter simulations within a large range of velocity dispersion, for the purpose of pointing out the effects on the formation of structure. We have then focused on a regime where the resolution is better balanced by the velocity distribution. Some of our findings are summarized below.

- In warm dark matter models, as our dark matter only simulations show, the structure formation follows a hybrid scenario in which both top-down and bottom-up scenarios have a saying.

- The early structure formation in this warm dark matter models is essentially top-down, with large halos forming in the highest density regions, tracked at the intersection of filaments. The second level of top down formation of structure is occurring along single isolated filaments.

- The biggest earlier formed halos will accrete matter from the filaments, while in small densities regions the mergers of smaller halos will result in a larger halo.

- Later on, and depending on the morphology of the region in which these halos formed, meaning mainly the density and the layout of the filaments, they merge into bigger halos creating a hierarchical build-up.

- The warm dark matter halos, especially the ones that did not suffer big mergers, show obvious shells and caustics.

- The warmer the dark matter the more pronounced is the top-down effect and the more delayed is the collapse.

- Albeit the numerical limitations we encounter as far as our warm dark matter simulations are concerned, we can conclude that an early top-down structure formation trend would be seen even in dark matter simulations with $v < 0.05$ km/s. For colder particles, this effect is hidden and wiped out by following abundant mergers resulting in a redshift zero distribution that seems in agreement with the hierarchical formation scenario.

- The number of small satellites, as previously found, is visibly reduced in the WDM simulations with respect to the CDM ones.

For a warm dark matter particle, as supported by the arguments adduced in Section 2, the thermal component of the velocity is important for different theoretical and practical considerations. The strong dependence of the mass-velocity relation on the actual particle production model makes it difficult to constrain certain properties of the dark matter particle, including its mass. The impact that a certain velocity dispersion is having on the structure formation and evolution on both small and large scales, as seen in simulations cannot be used as a strong constraint on the mass in the absence of a universal model for particle production. Furthermore, we have shown that there have been some inconsistencies in previous studies with respect to the use of velocities in the simulations, that lead to ambiguous results.

The baryonic physics may play an important role in the actual formation and evolution of halos, hence the necessity of further exploring these effects in simulations. High redshift observations of halos could be used in comparison with complex baryonic warm dark matter simulations in constraining the mass of warm dark matter particles based on their formation and merger history.

The baryonic processes that we have not included in the simulations must play an important role in the structure formation. Previously Gao & Theuns (2007) show a crucial difference in the collapse of a filament that contains both gas and dark matter in a 3 keV simulation, with respect to the cold dark matter case. In the WDM case, the stars form inside the filament, before the halo forms. This trend where stars form in filaments continues for 1.5 keV particles up to redshift $z \approx 2$ resulting in stringy ‘‘chain’’ galaxies that remain to be confirmed by observations (Gao, Theuns & Springel 2015).

The smoother space distribution in the warm dark matter scenario may allow baryons to condense coherently in a smooth potential halo, providing favorable conditions for forming disk-like galaxies. However, a much higher resolution than the one available in present simulations is needed to explore this effect.

ACKNOWLEDGMENTS

S.P. would like especially to thank Doug Potter and Joachim Stadel for their valuable input and help. Discussions with George Lake, Andrea Macciò, and Ben Moore are acknowledged.

REFERENCES

- Abazajian, K. & Koushiappas, S. M., 2006, *Phy.Rev.D*, 74, 023527
- Abel, T. and Hahn, O. and Kaehler, R., 2012, *MNRAS*, 427, 61
- Anderhalden, D., Diemand, J., Bertone, G., Macciò, A. V., Schneider, A., 2012, *JCAP*, 10, 47
- Atkins, P., Friedman, R. 2005, *Molecular Quantum Mechanics*, Oxford Univ. Press
- Bertschinger, E., 2001, *ApJS*, 137, 1
- Bode, P., Ostriker, J. P. & Turok, N., 2001, *ApJ*, 556, 93
- Bond, J. R., Efstathiou, G., Silk, J., 1980, *Phys. Rev. Let.*, 45
- Boyarsky, A., Ruchayskiy, O., Iakubovskiy, D., France, J., 2014, *Phys. Rev. Let.*, 113, 251301
- de Blok, W. J. G., McGaugh, S. S., Bosma, A., & Rubin, V. C. 2001, *ApJL*, 552, L23
- Bulbul, E. and Markevitch, M. and Foster, A. and Smith, R. K. and Loewenstein, M. and Randall, S. W., 2014, *ApJ*, 789, 13
- Chandrasekhar, S., 1942, *Principles of Stellar Dynamics*, The University of Chicago Press
- Colombi, S. and Dodelson, S. and Widrow, L. M., 1996, *ApJ*, 458, 1
- Cooper, A. P., Cole S., Frenk, C. S., White, S. D. M., Helly J., Benson, A. J., De Lucia, G., Helmi, A., et al., 2010, *MNRAS*, 406, 744
- Destri, C., de Vega, H. J. and Sanchez, N. G., 2013, *New Astronomy* 22, 39, arXiv:1204.3090
- Diemand, J. & Moore, 2010, B., *Particle Dark Matter: Observations, Models and Searches*, p. 14, (Cambridge University Press) (2010)
- Diemand, J. & Moore, B., 2011, *Advanced Science Letters*, 4, 297
- Gao, L. and Theuns, T., 2007, *Science*, 317, 1527
- Gao, L. and Theuns, T. and Springel, V., 2015, *MNRAS*, 450, 45
- Governato, F. and Weisz, D. and Pontzen, A. and Loebman, S. and Reed, D., Brooks, A. M., Behroozi, P., Christensen, C., Madau, P. and Mayer, L. and Shen, S. and Walker, M., Quinn, T., Keller, B. W., Wadsley, J., 2015, *MNRAS*, 448, 792
- Götz, M., Sommer-Larsen, J., 2002, *ApSS*, 281, 415
- Hahn, O., Angulo, R. E., 2015, arXiv:1501.01959
- Hansen, S. H., Lesgourgues, J., Pastor, S. & Silk, J., 2002, *MNRAS*, 333, 546
- Hénon, M., 1973, *Dynamical Structure and Evolution of Stellar Systems*, (Swiss Society of Astronomy and Astrophysics), p. 183
- Huang, K., *Statistical Mechanics*, 1987, John Wiley & Sons
- Kamada, A., Yoshida, N., Kohri, K., Takahashi, T., 2013, *JCAP*, 3, 8
- Klypin, A., Kravtsov, A. V., Valenzuela, O., & Prada, F. 1999, *ApJ*, 522, 82
- Kormendy, J., Drory, N., Bender, R., Cornell, M. E., 2010, *ApJ*, 723, 54
- Kuzio de Naray, R. & Kaufmann, T., 2011, *MNRAS*, 414, 3617
- Lin, C. C. and Mestel, L. and Shu, F. H., 1965, *ApJ*, 142, 1431
- Macciò A. V., Paduroiu S., Anderhalden D., Schneider A., Moore B., 2012, *MNRAS*, 424, 1105
- Marinacci F., Pakmor, R., Springel, V., 2014, *MNRAS*, 437, 1750
- Markovic Katarina, Viel Matteo, 2014, *Publications of the Astronomical Society of Australia*, 31, 6
- Martizzi, D., Teyssier, R., & Moore, B., 2013, *MNRAS*, 432, 1947
- Mashchenko, S., Wadsley, J., Couchman, H. M. P., 2008, *Science*, 319, 174
- Melott, A., L., 2007, arXiv:0709.0745
- Miller, R.H., 1964, *ApJ*, 140, 250
- Moore, B., Ghigna, S., Governato, F., Lake, G., Quinn, T., Stadel, J., & Tozzi, P. 1999, *ApJL*, 524, L19
- Muccione, V., Pfenniger, D., 2006, *EAS Publications Series*, 20, 291
- Navarro, J. F., Frenk, C. S., & White, S. D. M., 1996, *ApJ*, 462, 563
- Padmanabhan, T., *Theoretical Astrophysics*, Vol. III (Cambridge University Press)
- Peacock, J., *Cosmological Physics* (Cambridge University Press)
- Peebles, P. J. E., 1993, *Principles of Physical Cosmology* (Princeton Univ. Press)
- Pfenniger, D. and Muccione, V., 2006, *A&A*, 456, 45
- Pierpaoli, E. and Borgani, S. and Masiero, A. and Yamaguchi, M., 1998, *Phy.Rev.D*, 57, 2089
- Pontzen A., Governato F., 2012, *MNRAS*, 421, 3464
- Salucci, P., Wilkinson, M. I., Walker, M. G., Gilmore, G. F., Grebel, E. K., Koch, A., Frigerio Martins, C., Wyse, R. F. G., 2012, *MNRAS*, 420, 2034
- de Souza, R. S., Mesinger, A., Ferrara, A., Haiman, Z., Perna, R., Yoshida, N., 2013, *MNRAS*, 432, 3218
- Schneider, A. and Smith, R. E. and Reed, D., 2013, *MNRAS*, 433, 1573
- Seljak, U., Makarov, A., McDonald, P., & Trac, H., 2006, *Phys. Rev. Let.*, 97, 191303
- Springel, V., 2005, *MNRAS*, 364, 1105
- Stadel, J., 2001, PhD Thesis, University of Washington
- Stadel J., Pooter, D., Moore, B., Diemand, D., Madau, P., Zemp, M., Kuhlen, M. & Quilis, V., 2009, *MNRAS*, 391, L21
- Trodden, M., Carroll, S.M., 2004, arXiv:0401547
- de Vega, H. J. and Sanchez, N. G., 2011, arXiv:1109.3187
- de Vega, H. J. and Falvela, M. C. and Sanchez, N. G., 2012, arXiv:1203.3562
- Viel, M., Lesgourgues, J., Haehnelt, M. G., Matarrese, S., & Riotto, A., 2005, *Phy.Rev.D*, 71, 063534
- Wang, J., White, S. D. M., 2007, *MNRAS*, 380, 93
- Weinberg, S., 1962, *Phys.Rev.*, 128, 1457
- Weinberg, S., 2008, *Cosmology*, Oxford Univ. Press
- Zel'dovich, Y. B., 1970 *A&A*, 5, 84

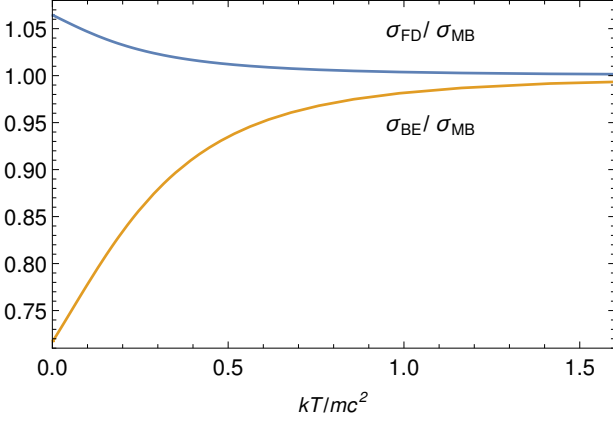


Figure A1. The ratios between the velocity dispersions $\sigma_{\text{FD}}/\sigma_{\text{MB}}$ and $\sigma_{\text{BE}}/\sigma_{\text{MB}}$ with respect to the temperature

APPENDIX A: VELOCITY DISPERSION DEPENDENCE ON TEMPERATURE IN FERMI-DIRAC AND BOSE-EINSTEIN DISTRIBUTIONS

As mentioned in Sect. 2.2.1, we check the correction to velocity dispersion that should be applied to a Maxwell-Boltzmann distribution when the physical system follows a given quantum statistics.

The energy of a particle as a function of momentum p , valid in all regimes (relativistic and non-relativistic), is

$$\epsilon(p) = \sqrt{p^2 c^2 + m^2 c^4} - mc^2, \quad (\text{A1})$$

and the velocity

$$v(p) = \frac{pc}{\sqrt{m^2 c^2 + p^2}}. \quad (\text{A2})$$

The corresponding 1D spherical distributions for Fermi-Dirac, Maxwell-Boltzmann and Bose-Einstein cases are:

$$f_{\text{FD}} = \frac{4\pi p^2}{\exp(\epsilon(p)/kT) + 1} \quad (\text{A3})$$

$$f_{\text{MB}} = \frac{4\pi p^2}{\exp(\epsilon(p)/kT)} \quad (\text{A4})$$

$$f_{\text{BE}} = \frac{4\pi p^2}{\exp(\epsilon(p)/kT) - 1} \quad (\text{A5})$$

Integrating over all p , we obtain the normalization constant

$$S = \int_0^\infty f dp. \quad (\text{A6})$$

For each case respectively the second moment are

$$\sigma_{\text{FD}}^2 = \frac{1}{S} \int_0^\infty p^2 f_{\text{FD}} dp, \quad (\text{A7})$$

$$\sigma_{\text{MB}}^2 = \frac{1}{S} \int_0^\infty p^2 f_{\text{MB}} dp, \quad (\text{A8})$$

$$\sigma_{\text{BE}}^2 = \frac{1}{S} \int_0^\infty p^2 f_{\text{BE}} dp. \quad (\text{A9})$$

Computing these integrals by numerical quadrature, we find

the ratios between the velocity dispersions $\sigma_{\text{FD}}/\sigma_{\text{MB}}$ and $\sigma_{\text{BE}}/\sigma_{\text{MB}}$ with respect to temperature. The result is plotted in Fig. A1. In any situation the Fermi-Dirac velocity dispersion is not significantly different from Maxwell-Boltzmann's, differing by at most $\sim 6.5\%$, while the Bose-Einstein velocity dispersion differs more, up to $\sim 27\%$. The highest differences occur at low temperature, corresponding to low redshifts. This is not such a dramatic correction as the factor 3.571 invoked in Macciò et al. (2012), but can still be significant for high precision cosmology works.

APPENDIX B: DETAILED DERIVATION OF THE RESULTS IN SECTION 2.2.2

Using these expressions inserted into Eq. (19), the specific particle entropy becomes

$$\frac{s}{k} = \frac{1}{3} \frac{\int_0^\infty \frac{y^{3/2} \sqrt{2q+y} (5q+4y)}{Z^{-1} \exp(y) \pm 1} dy}{\int_0^\infty \frac{y^{1/2} \sqrt{2q+y} (q+y)}{Z^{-1} \exp(y) \pm 1} dy} - \ln(Z), \quad (\text{B1})$$

where $Z \equiv \exp(\mu/kT)$, $q \equiv mc^2/kT$ and $y \equiv (\sqrt{p^2 c^2 + m^2 c^4} - mc^2)/kT$. Thus s is a function of the reduced dimensionless variables Z and q only, and not of g , m and physical constants explicitly.

In the ultra-relativistic regime when the energy of particles is comparable or higher than the rest mass energy, particles and their antiparticles can be created in equal number, so any chemical potential should cancel to a high degree. Then s/k at $\mu = 0$ becomes a constant. The closed form expressions are,

$$\lim_{T \rightarrow \infty} \frac{s(T, 0)}{k} = \frac{7}{135} \frac{\pi^4}{\zeta(3)} \approx 4.20183245, \quad (\text{B2})$$

for fermions, and

$$\lim_{T \rightarrow \infty} \frac{s(T, 0)}{k} = \frac{4}{45} \frac{\pi^4}{\zeta(3)} \approx 3.60157071, \quad (\text{B3})$$

for bosons, where ζ is Riemann's function, and $\zeta(3) \approx 1.20205690$.

The particle velocity at all regimes can be derived from the relativistic particle kinetic energy $\epsilon(T, \mu) = e(T, \mu)/n(T, \mu) = \sqrt{p^2 c^2 + m^2 c^4} - mc^2$ and that relativistic momentum is related to velocity by $v^2/c^2 = 1/(1+m^2 c^2/p^2)$. Eliminating p yields, noting $Y \equiv \epsilon/mc^2$,

$$\frac{v^2(T, \mu)}{c^2} = 1 - \frac{1}{(1+Y)^2} = \frac{Y(2+Y)}{(1+Y)^2}. \quad (\text{B4})$$

The second form is numerically more precise at low energy. The non-relativistic and ultra-relativistic expansions read, respectively,

$$\frac{v^2}{c^2} \approx 2Y - 3Y^2 + 4Y^3 - \dots \quad (\text{B5})$$

$$\frac{v^2}{c^2} \approx 1 - Y^{-2} + 2Y^{-3} - 3Y^{-4} + \dots \quad (\text{B6})$$

As stated in Section 2.2.2, the conserved particle density $n(T, \mu)$ is related to universal expansion by the scale factor $a = 1/(1+z)$ and therefore

$$n(T(z), \mu(z)) = n_0(1+z)^3, \quad (\text{B7})$$

APPENDIX C: MOVIES CAPTIONS AND SNAPSHOTS

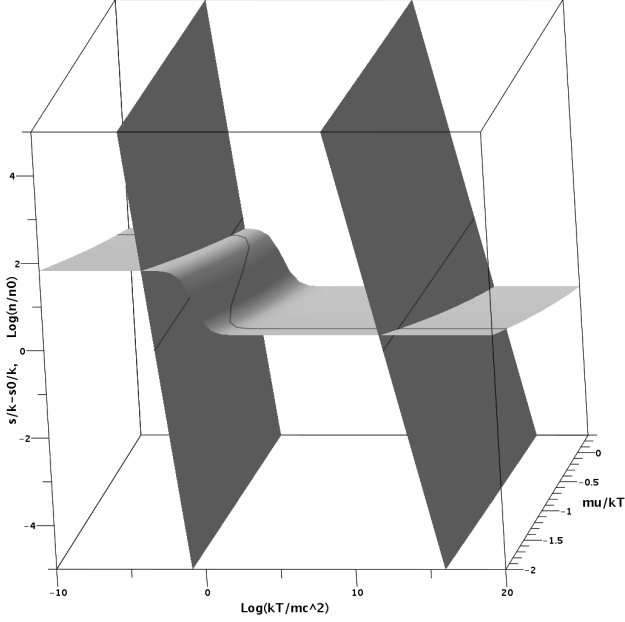


Figure B1. Density n and entropy s/k as functions of temperature T and chemical potential μ as given in Eq. (B7) and (B8). The light-grey surface is the entropy and the dark-grey ones are the density at two redshifts $z = 10^9$ on the left (relativistic), and $z = 0$ on the right (non-relativistic), while $n_0 = 115 \text{ cm}^{-3}$, $g = 1$, and $m = 1 \text{ keV}/c^2$. The intersection of the level curves yields the solution of Eq. (B7) and (B8).

while the constant particle entropy gives

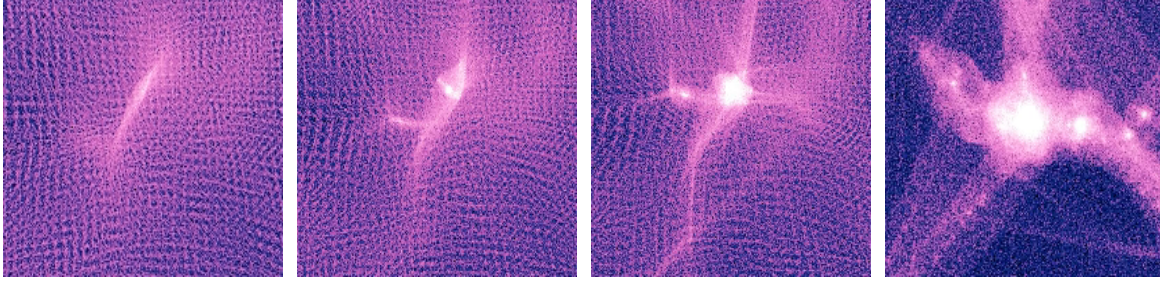
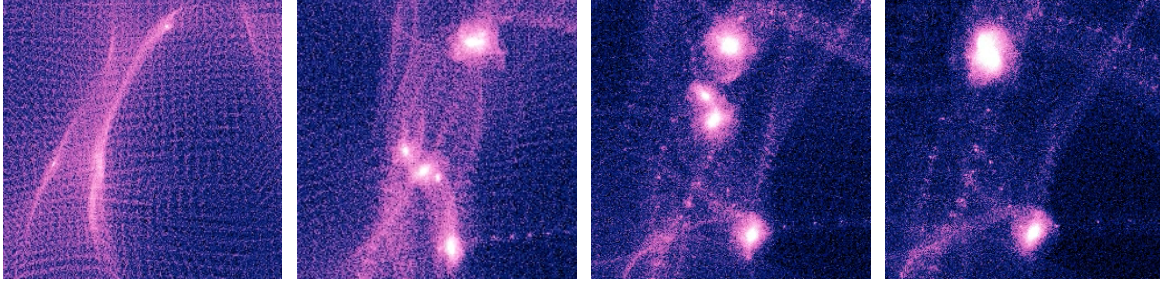
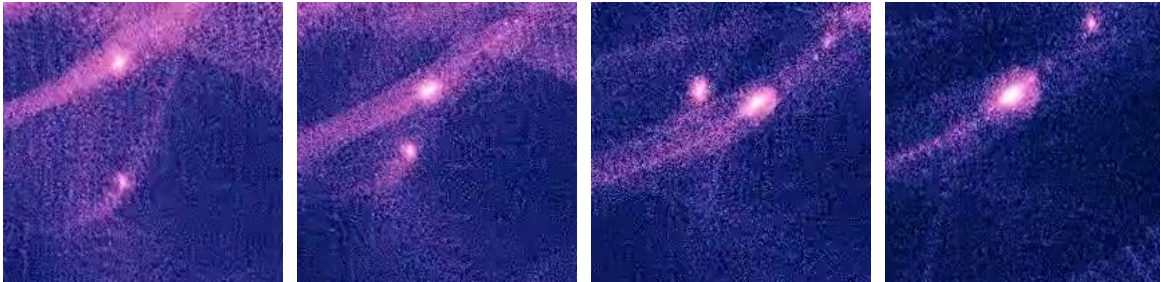
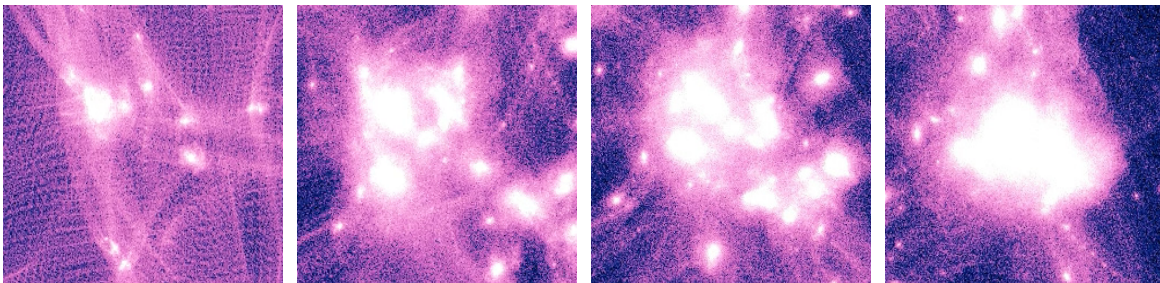
$$\frac{s(T(z), \mu(z))}{k} = \frac{s(\infty, 0)}{k} = 4.20183245, \quad (\text{B8})$$

For a given particle density n_0 , redshift z and particle mass m the non-linear Eq. (B7) and (B8) can be solved with a non-linear equation solver for T and μ . The functions are univalued and level curves of n and s intersect once, so any combination of T and μ gives a single solution (see Fig. B1). Actually the constant level curves n and s expressed with the variables $\log q$ and Z intersect almost at right angle: $n(\log q, Z)$ depends most rapidly on $\log q$, and $s(\log q, Z)$ depends most rapidly on Z , so finding a solution for $\log q$ for n at constant Z and then a solution for Z at constant q for s , and repeating until satisfaction could be a method to find a solution. Since the thermodynamic functions involve integrals, a fast numerical integrator is handy, since several indefinite integrals must be evaluated at each iteration. To perform this we used Maple 18 which includes a non-linear multidimensional function root solver, and evaluate quickly numerical integrals with the NAG library algorithm D01AMC.¹¹ When T and μ are found for a given particle mass and degeneracy factor g , all the other quantities like v^2 can be derived by plugging these values in the functions, which may require again few numerical integral evaluations. The results are presented in Section 2.2.2.

¹¹ The Maple script is available on request.

Table C1. Description of the movies accompanying the paper

Label	Description
cosmoboxvel.avi	Movie of full-box WDM2 simulation
cosmoboxall.avi	WDM1 and WDM2 full-box simulations side-by-side showing the effect of thermal velocities
lu.avi ld.avi ru.avi rd.avi	A zoom in the 1/4 of the WDM2 simulation
halo.avi	A $7 \times 10^{12} M_{\odot}$ 18×10^6 particles high-resolution refined halo from WDM5
halozoom.avi	A zoom in the refined halo focused on the central region where the shells and caustics can be observed

**Figure C1.** A zoom in a region from the WDM2 simulation, showing the evolution of a halo which forms top-down at the intersection of the filaments and then starts accreting matter**Figure C2.** A zoom in a region from the WDM2 simulation showing how small halos formed later that merge hierarchically in a larger halo**Figure C3.** An early formed halo which doesn't suffer mergers**Figure C4.** A large high density region with many filaments where the halos formed early on via top-down collapse are merging in a violent manner creating a larger cluster